VERSION OCTOBER 7, 2022
Preprint typeset using LaTeX style openjournal v. 09/06/15

PANCO2: A PYTHON LIBRARY TO MEASURE INTRACLUSTER MEDIUM PRESSURE PROFILES FROM SUNYAEV-ZELDOVICH OBSERVATIONS

F. KÉRUZORÉ[1,2,⋆], F. MAYET[2], E. ARTIS[2], J.-F. MACÍAS-PÉREZ[2], M. MUÑOZ-ECHEVERRÍA[2], L. PEROTTO[2], F. RUPPIN[3], AND OTHERS?
[1]High Energy Physics Division, Argonne National Laboratory, 9700 South Cass Avenue, Lemont, IL 60439, USA
[2]Univ. Grenoble Alpes, CNRS, Grenoble INP, LPSC-IN2P3, 53, avenue des Martyrs, 38000 Grenoble, France
[3]Univ. Lyon, Univ. Claude Bernard Lyon 1, CNRS/IN2P3, IP2I Lyon, F-69622, Villeurbanne, France
Version October 7, 2022

ABSTRACT

We present panco2, an open-source Python library designed to fit pressure profiles in Sunyaev-Zeldovich maps. The fitting procedure is based on forward modeling of the total observed signal, allowing to take into account usual features of millimeter observations, such as beam smearing, data processing filtering, and point source contamination. panco2 offers a large flexibility in the inputs that can be handled and the analysis options, enabling refined analyses and studies of systematic effects. We detail the functionalities of the code, the algorithm used to infer pressure profile measurements, and the typical data products. We present examples of running sequences, and the validation on simulated inputs. The code is available on github, and comes with an extensive technical documentation to complement this paper.

Subject headings: Cosmology: large-scale structure of Universe

1. INTRODUCTION

Galaxy clusters are deeply interesting physical objects. Their abundance in mass and redshift is tightly linked to cosmic evolution, and can therefore be used as a cosmological probe (see *e.g.* Allen et al. 2011, for a review). In order to exploit this property, large sky surveys have been used to build catalogs of serendipitously detected clusters at different wavelengths, such as X-rays (*e.g.* Liu et al. 2022), optical (*e.g.* DES Collaboration et al. 2020), and millimeter-waves (*e.g.* Bleem et al. 2020).

Among these, one of the wavelengths of choice for the detection of galaxy clusters is the millimeter domain. Clusters can be observed at such frequencies through the Sunyaev-Zeldovich effect (SZ, Sunyaev & Zeldovich 1972), *i.e.* the spectral distortion of the cosmic microwave background (CMB) due to the Compton scattering of its photons on the free electrons of gas along the line of sight. The SZ effect is often separated in different components, depending on the origin of the energy transferred from the electrons; the main components being, by order of decreasing importance, the thermal (tSZ) and kinetic (kSZ, Sunyaev & Zeldovich 1980) effects (see Mroczkowski et al. 2019, for a recent review of the SZ effects). Catalogs of clusters detected through their tSZ signal are particularly interesting for cosmological applications, as the amplitude of the tSZ effect does not suffer from cosmological dimming (Carlstrom et al. 2002). As a result, modern millimeter-wave sky surveys have brought us some of the largest and deepest cluster samples to date, with the catalogs built from the Atacama Cosmology Telescope (ACT, Hilton et al. 2021), the South Pole Telescope (SPT, Bleem et al. 2020), and *Planck* (Planck Collaboration et al. 2016a) surveys.

The amplitude of the tSZ distortion is directly proportional to the electron pressure in the gaseous intracluster medium (ICM) integrated along the line of sight. This link between tSZ signal and ICM pressure motivates studies of the pressure distribution in the ICM – in its simplest form, as a spherically symmetric pressure profile. For example, matched-filtering cluster detection algorithms may require a prior assumption on the overall shape of the ICM pressure profile (*e.g.* Melin et al. 2012), in which case a poor knowledge of this property of clusters may lead to a poorly constructed cluster sample. Similarly, the power spectrum of the tSZ effect on the sky, which can be used to constrain cosmology, strongly relies on an assumption of the pressure profile of clusters, and the recovering of cosmological parameters can be severely affected by its poor knowledge (Ruppin et al. 2019). The mean pressure profile of galaxy clusters has been investigated using different cluster samples over the last decade. Early works conducted on local, X-ray selected samples, such as Arnaud et al. (2010, hereafter A10), converged towards a "universal" pressure profile, undergoing self-similar redshift and mass evolution (see also *e.g.* Battaglia et al. 2012; Planck Collaboration et al. 2013) In these studies, the main determining factor for the shape of the pressure profile of a cluster was its dynamical state, with relaxed clusters exhibiting a steeper pressure profile in their core. Nevertheless, the pressure profile of clusters is expected to deviate from self-similarity because of various baryonic processes, such as feedback by active galactic nuclei jets and supernovae explosions. The impact of these processes is still largely unknown, as they are expected to have a larger importance in the shallower gravitational potentials of low-mass halos, which are harder to detect and study observationally. To better understand these impacts, large efforts are made to produce hydrodynamical simulations with a rich description of baryonic physics, but these in turn need to calibrate their subgrid models on observation-based studies, making the measurement of pressure profiles from observations a key element of studies of cluster physics and cosmology.

The first step in any evaluation of the mean pressure profile of a sample is the extraction of individual profiles from observed data. Such measurements can be performed from X-ray cluster observations, using a deprojection of the ICM electron density and temperature (see *e.g.* Böhringer & Werner 2010; Böhringer & Schartel 2013, for reviews). Because of cosmological dimming, the X-ray surface brightness measure towards a cluster – at fixed density – strongly decreases with

⋆E-mail:fkeruzore@anl.gov

redshift, with $S_X \propto (1+z)^{-4}$. As a consequence, X-ray observations of sufficient depth to infer quality measurements of pressure profiles can be prohibitively costly from an observation time perspective for high redshift systems. Alternatively, one may use tSZ observations of clusters, which do not suffer from this redshift dimming, enabling the detection of more distant objects. In particular, high angular resolution millimeter observations of clusters with large aperture telescopes have successfully been used to measure cluster pressure profiles, and are today one of the preferred sources of data for studies of the mean pressure profile of clusters (*e.g.* Mayet et al. 2020; Young et al. 2022; Sayers et al. 2022).

In this paper, we present `panco2`, a `Python` library written to perform pressure profile extraction from tSZ observations. The algorithm is based on forward modeling of the tSZ signal and MCMC sampling, and allows users to account for different features of millimeter-wave observations that may manifest as systematic biases or uncertainties in recovered pressure profiles. An earlier version of `panco2` was described in Kéruzoré et al. (2021), which offered less flexibility in the analysis, as the only data that could be analyzed was maps from the NIKA2 camera 150 GHz channel (Adam et al. 2018; Perotto et al. 2020). This software has already been used for different studies based on NIKA2 data (*e.g.* Artis et al. 2022; Muñoz-Echeverría et al. 2022a,b). Here, we present a generalization of the code, that makes it able to perform pressure profile extractions from arbitrary data formats.

The paper is structured as follows **[todo: .]** Suspendisse vel felis. Ut lorem lorem, interdum eu, tincidunt sit amet, laoreet vitae, arcu. Aenean faucibus pede eu ante. Praesent enim elit, rutrum at, molestie non, nonummy vel, nisl. Ut lectus eros, malesuada sit amet, fermentum eu, sodales cursus, magna. Donec eu purus. Quisque vehicula, urna sed ultricies auctor, pede lorem egestas dui, et convallis elit erat sed nulla. Donec luctus. Curabitur et nunc. Aliquam dolor odio, commodo pretium, ultricies non, pharetra in, velit. Integer arcu est, nonummy in, fermentum faucibus, egestas vel, odio.

Throughout this paper, even though `panco2` can use different cosmologies, we assume a flat ΛCDM model, with $\Omega_\mathrm{m} = 0.3$, $\Omega_\Lambda = 0.7$, $h = 0.7$. This cosmology is mainly used to infer angular diameter distances to the cluster being studied from its redshift, in order to accurately map sky distances to physical ones. Quantities with a 500 subscript refer to the properties of a cluster within its characteristic radius R_{500}, corresponding to the radius of a sphere around the center of the cluster in which the mean matter density is 500 times the critical density of the Universe at the cluster's redshift.

2. ALGORITHM

The goal of `panco2` is to infer a measurement of a pressure profile and of its confidence intervals from the SZ map of a cluster. The overall workflow implemented in `panco2` to perform this measurement is presented in Figure 1. It is based on the forward modeling of the SZ map and on Monte-Carlo Markov Chain (MCMC) sampling of the probability distribution for the pressure profile parameters given the input data. In this section, we detail each step of the analysis, as well as the inputs to be given to `panco2` and the results it produces.

2.1. *Data inputs*

The main input of `panco2` is a mapping of a patch of the sky containing SZ signal. The code uses the FITS standard (Wells et al. 1981) to correctly map sky coordinates to pixels using the flat-sky approximation. The map to be fitted must therefore be contained within a FITS file, that must include the following ingredients:

- An extension in which the data is the SZ map to be fitted, and the header includes the World Coordinate System (WCS) used to create the map;
- An extension in whichs the data represent an estimate of the expected root mean squared (RMS) error for each pixel of the data map.

Such a file constitutes the minimum data input for `panco2` to proceed fitting a pressure profile. Using these inputs, the user may choose to only use a square portion of the map, by specifying the sky coordinates of its center and its side.

Additional inputs can be provided to account for various data features.

Beam smearing — the user may provide the width of a Gaussian function to account for point spread function (PSF, hereafter referred to as "beam") filtering (see §2.3);

Transfer function — Fourier filtering due to data processing and/or scanning strategy can be accounted for in the analysis (see §2.3);

Point source contamination — the position on the sky of point sources, as well as their fluxes and uncertainties, can be used to account for the contamination and marginalize over its amplitude (see §2.3);

Correlated noise — the covariance matrix between the noise of pixels in the map can be provided (see §2.4). `panco2` also offers routines to compute the covariance from various data inputs, such as the power spectrum of the residual noise;

Integrated SZ signal — an external measurement of the integrated Compton parameter, that may be used as a constraint on large-scale tSZ signal, can be given to `panco2` (see §2.4).

2.2. *Pressure profile model*

The electron pressure distribution in the ICM is modeled in `panco2` as a radial pressure profile, implying spherical symmetry of the ICM. The most widely used parametrization for ICM pressure profiles, called the generalized Navarro-Frenk-White model (gNFW, Zhao 1996; Nagai et al. 2007), is known to have several shortcomings. In particular, the very self-constrained shape of the functional form of the profile and the important correlations in the parameter space make model fitting complex, and the recovered parameter values hard to interpret (see *e.g.* Nagai et al. 2007; Battaglia et al. 2012; Sayers et al. 2022).

In order to try to circumvent these issues, `panco2` uses a more flexible parametrization of the pressure profile, in which the pressure distribution is modeled as a power law evolution in concentric spherical shells. In this modeling, the model parameters are the values P_i of the pressure profile at predefined radii from the cluster center R_i, with a power law interpolation between the radii [1]:

$$P(r \in [R_i, R_{i+1}[) = P_i \, (r/R_i)^{-\alpha_i}\,, \tag{1}$$

[1] Several papers in the literature have dubbed this modeling a "non-parametric" approach; as this may induce confusion, since the model is parametric, we will refrain from using this term, and refer to our model as "radially binned".

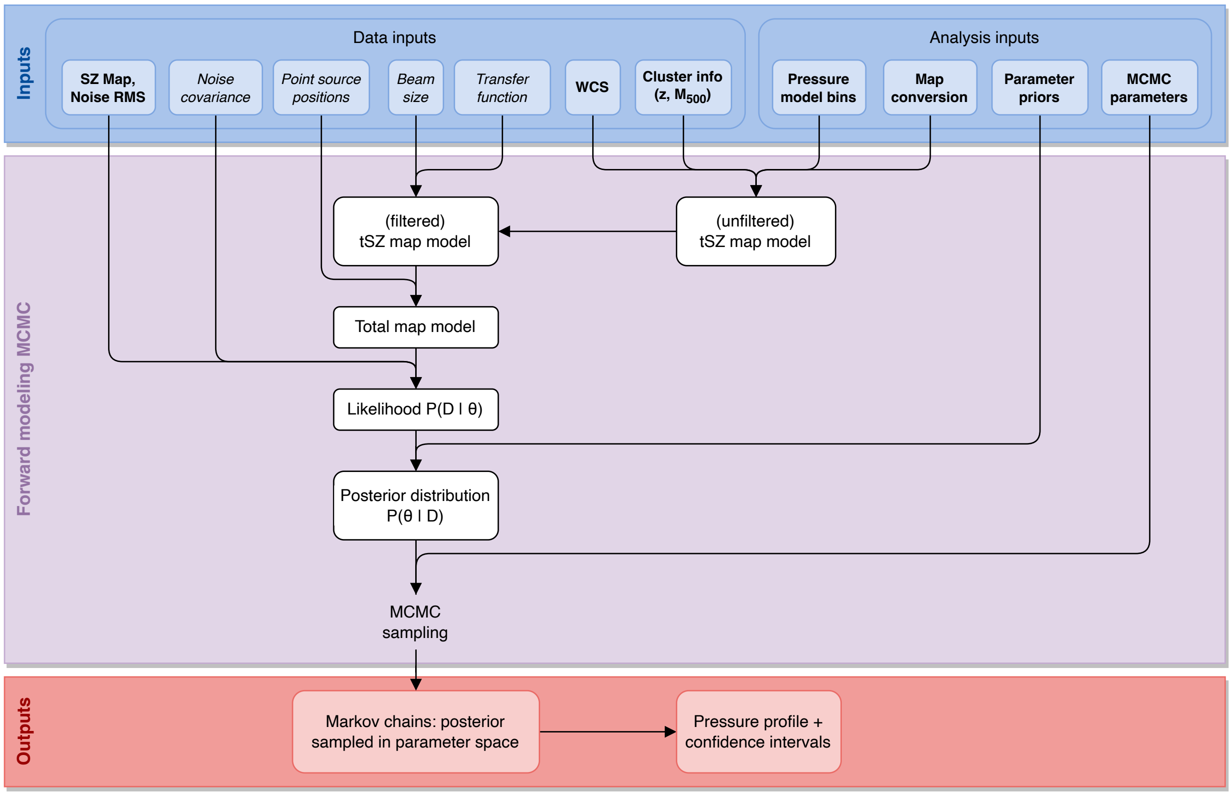

FIG. 1.— Schematic workflow of the panco2 algorithm, from its inputs (blue), to the forward modeling and MCMC sampling (purple), and results (red). Required and optional inputs are denoted with boldface and italic fonts, respectively.

where $\alpha_i = -\log(P_{i+1}/P_i)/\log(R_{i+1}/R_i)$.
Outside the radial bins, the pressure profile is extrapolated using the power-law evolution of the first (last) bin. In addition to being more flexible and having generally lesser correlations in the parameter space, this parametrization can be integrated along a line of sight analytically through Abell transform, by following *e.g.* Romero et al. (2018).

The main downside to this pressure profile modeling lies in the need to specify the radii R_i used in eq. (1) *a priori* when performing a fit. There is no obvious, fail-safe way to define this radial binning. A user may choose a binning motivated by the data coverage (*e.g.* with radii that, projected on the sky plane, are separated the beam of the instrument used to build the map); but looking at the same data, another user may be motivated by sample studies over several clusters, and wish to define a binning in units of a characteristic radius of the cluster (*e.g.* R_{500}). As a result, model dependence may arise in the results produced by panco2. This point will be addressed in §5.

2.3. *Forward modeling: from pressure profile to SZ map*

The approach used by panco2 to fit pressure profiles on SZ maps is forward modeling. In that framework, a pressure profile model – determined by eq. (1) – is used to generate a map that can be compared to data. This approach has been vastly used in the estimation of pressure profiles from tSZ maps, especially in the context of resolved follow-up of galaxy clusters with *e.g.* NIKA2 (*e.g.* Muñoz-Echeverría et al. 2022a; Kéruzoré et al. 2020), MUSTANG(2) (*e.g.* Romero et al. 2017, 2020), Bolocam (*e.g.* Sayers et al. 2022), or ALMA (*e.g.* Di Mascolo et al. 2019). This section details the different steps used in that process, which is illustrated in figure 2.

Line of sight integration — The amplitude of the tSZ effect in a direction θ on the sky is named the Compton parameter y, and is proportional to the integral along of the electron pressure along the line of sight (LoS):

$$y(\theta) = \frac{\sigma_{\text{T}}}{m_{\text{e}}c^2} \int_{\text{LoS}(\theta)} P_{\text{e}} \, \text{d}l, \quad (2)$$

where σ_{T} is the Thompson cross-section, and $m_{\text{e}}c^2$ is the electron resting energy.
In panco2, we perform this integration analytically, by following the derivation presented in Appendix A of Romero et al. (2018), using the spherically symmetric case (in the notation of Romero et al., $a_i = b_i = c_i = 1 \; \forall \; i$). This allows us, for any given pressure profile, to create a Compton parameter map in the same coordinate system as the data, *i.e.* an estimate of the value of y for each pixel in the map.

Conversion and zero level — Depending on the data product available, and on the convention used in the raw data processing software employed to create these data products, tSZ maps can have a variety of units (*e.g.* surface brightness, CMB temperature fluctuation). These units can usually be converted to Compton$-y$ through a scalar conversion coefficient, C_{conv}, which can depend on many different quantities that may be difficult to estimate, or even fluctuate during observations, such as instrumental bandpasses, weather conditions, instrumental calibration, or even temperature of the ICM through relativistic corrections to the tSZ effect (Mroczkowski et al. 2019). As a result, the conversion coefficient is affected by an uncertainty. In panco2, this coefficient is treated as a parameter in the model, for which a prior distribution needs to be specified (see §2.5), allowing to propagate the uncertainty on the con-

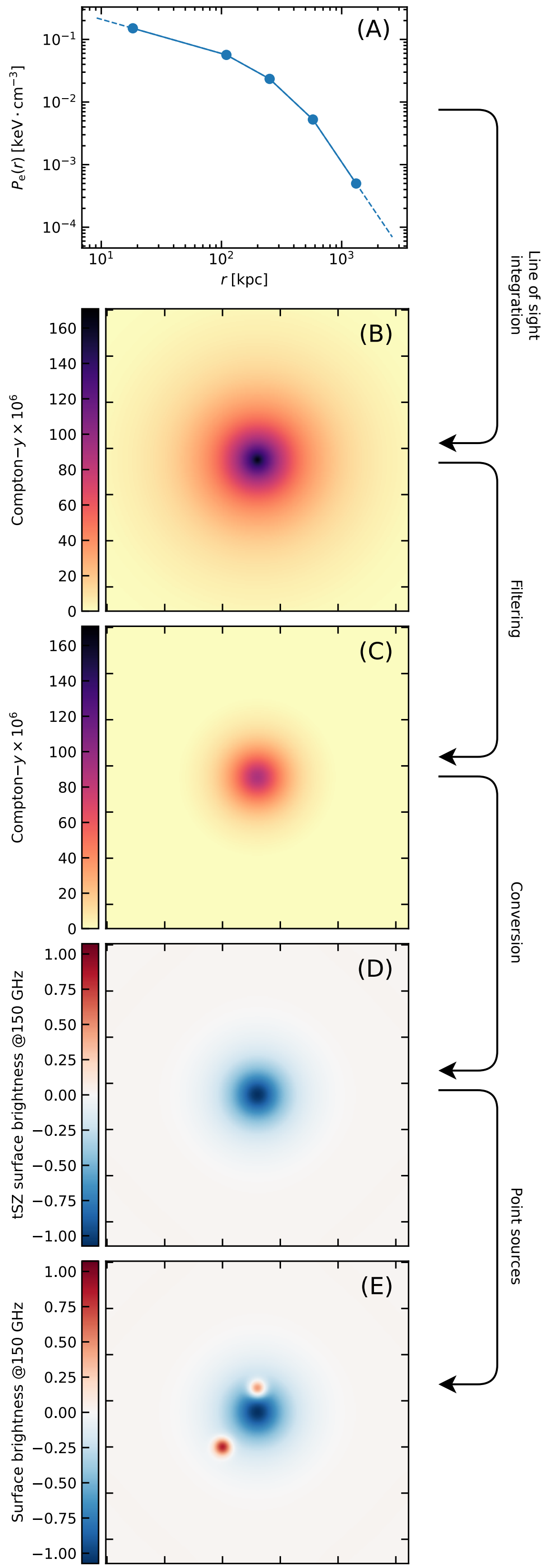

FIG. 2.— Illustration of the forward modeling procedure. The pressure profile (A) is integrated along the line of sight to create a Compton$-y$ map (B), which is filtered (C) and converted (D) to be realistically comparable to the observed data. If point source contamination information is passed, point source models can be added to the map (E).

version of the map to the pressure profile estimate. This means that a vector in the parameter space will contain a value of a conversion coefficient, which `panco2` multiplies the model $y-$map by to get a map in the same units as the input data. In case the input data is already in units of Compton$-y$, this coefficient may still be used to propagate multiplicative calibration uncertainty by centering the prior distribution on 1. In addition, in order to enable taking into account possible large-scale residual noise, a zero-level offset can be added to the map, and marginalized over.

Filtering — The tSZ maps constructed by any instrument are affected by different types of filtering. The instrumental PSF acts as a filter that smooths the data by suppressing signal at small scales. In its forward modeling approach, `panco2` is able to take into account this filtering by convolving the model $y-$map with a 2D Gaussian filter, the width of which can be specified by the user.

In addition, during the data reduction process used to create tSZ maps from raw data, filtering can occur, often suppressing signal at large angular scales. This filtering is usually accounted for through a transfer function, quantifying the signal filtering in the Fourier space, and evaluated during the data processing. `panco2` can account for this effect by filtering the map with a transfer function provided by the user. Two different types of transfer functions can be provided: **[todo: I want to make the code use ℓ, not k. Correct this when done.]**

- a 1D transfer function: assuming that the filtering is isotropic, `panco2` can convolve model maps with a 1D kernel specified by the user as angular frequencies k and their associated filtering $\mathrm{TF}(k)$;
- a 2D transfer function: if the filtering on the sky cannot be assumed to be isotropic, the user may specify 2D angular scales (k_x, k_y) and their corresponding filter $\mathrm{TF}(k_x, k_y)$.

A thorough discussion of the impact of choosing a 1D or 2D transfer function – in the case of NIKA2 data, in which the filtering is mildly anisotropic – can be found in Muñoz-Echeverría et al. (2022a).

Point source contamination — After applying the different filters, the `panco2` model map is a map of the tSZ signal, in the unit and mapping as the input data, and having been affected by the same signal filtering. It is therefore comparable to the tSZ signal in the input map. But millimeter-wave maps of cluster regions may also include astrophysical signal from other sources. In particular, signal from millimeter-emitting galaxies can often be found in such maps. These galaxies can be foreground, background, or cluster members, and their emission can be thermal (in the case of dusty star-forming galaxies), or synchrotron (for radio-loud AGN). In any case, this signal manifests as a contamination for tSZ science, and must be accounted for in data analysis, lest the recovered pressure profile be biased.

In its forward modeling approach, `panco2` uses the methodology described in *e.g.* Kéruzoré et al. (2020), in which point source models may be added to the tSZ model map in order to model the total signal in the map. The spatial model of each source is given by the instrumental PSF, and their fluxes are treated as model parameters, with priors specified by the user (see §2.5). If the flux of a source is well known from external data, this prior will be tight, and serve as a propagation of its uncertainty to the recovered pressure profile. Otherwise, if a source is known to be present but little is known about its flux, large priors can be used, in which case panco2 will constrain the sum of the tSZ signal and the point source flux[2]. To account for point source contamination in the analysis, the user must therefore provide panco2 with a position (in sky coordinates) and a probability distribution for the flux (in input map units) for each of the sources considered.

2.4. *Likelihood*

The process described in §2.3 allows panco2 to compute a model map that is comparable to the input data from any position in the parameter space. To summarize, a vector in this parameter space, ϑ, has the following components:

- $P_0, \dots P_n$: the value of the pressure profile at each predefined radius $R_0, \dots R_n$;
- $C_{\rm conv}$: the conversion coefficient from Compton$-y$ to input map units;
- Z: a zero-level for the map;
- If provided, $F_0, \dots F_m$: the fluxes of point sources in the map, in input map units.

The comparison between the model map and the input data is performed through a Gaussian likelihood function:

$$\begin{aligned} -2 \log \mathcal{L}(\vartheta) &\equiv -2 \log p(D|\vartheta) + \text{cst.} \\ &= \left[D - M(\vartheta)\right]^{\rm T} \mathbf{C}^{-1} \left[D - M(\vartheta)\right], \end{aligned} \tag{3}$$

where D is the input map, $M(\vartheta)$ is the model map computed from the position in parameter space ϑ, and $\mathbf{C}$ is the noise covariance matrix.
If the noise in the map can be considered white, the noise values in the map pixels are uncorrelated, and $\mathbf{C}$ becomes diagonal. In that case, in order to reduce the computation time needed, the likelihood is rewritten as:

$$-2 \log \mathcal{L}(\vartheta) = \sum_i \left(\frac{D_i - M_i(\vartheta)}{\Sigma_i}\right)^2, \tag{4}$$

where the sum runs over all pixels i in the map, and Σ is the noise RMS map.

In some cases, especially with high angular resolution follow-ups of clusters, additional information may be known from SZ surveys, such as the integrated tSZ signal $Y_{<R}$ within a radius R of the cluster. This knowledge can serve as an additional constraint on the model, by computing the value of the integrated tSZ signal from the model as the spherical integration of the pressure profile within the radius R. This value can then be compared to that known from independent measurement, providing an additional data point that can be added to the log-likelihood of eqs. (3 or 4):

$$\left(\frac{Y^{\rm meas.}_{<R} - \frac{\sigma_{\rm T}}{m_{\rm e}c^2}\int_0^R P_{\rm e}(r)\, r^2 {\rm d}r}{\Delta Y^{\rm meas.}_{<R}}\right)^2, \tag{5}$$

where $Y^{\rm meas.}_{<R}$ and $\Delta Y^{\rm meas.}_{<R}$ are the measured integrated SZ signal within R and its uncertainty.

[2] panco2 is able to constrain the sum of the two because of the different spatial distribution of the tSZ and point source fluxes.

This additional constraint can be especially useful when dealing with observations agressively filtering large scale signal, in which case it might effectively provide constraining power on the pressure profile at large radii. This approach is routinely used for NIKA2 tSZ follow-ups of SZ-detected clusters (*e.g.* Ruppin et al. 2018; Kéruzoré et al. 2020; Muñoz-Echeverría et al. 2022a).

2.5. *Posterior distribution and MCMC sampling*

panco2 performs the extraction of pressure profile from tSZ data using Bayesian MCMC. In that framework, a prior probability distribution for the parameters, $p(\vartheta)$, must be multipled to the likelihood function of eq. (3) to obtain a posterior distribution for the parameters given the data: $p(\vartheta|D) \propto p(D|\vartheta)\, p(\vartheta)$. In panco2, the prior distributions for the different model parameters are considered uncorrelated, meaning the prior distribution is the product of the individual priors on parameters:

$$p(\vartheta) = \prod_i p(\vartheta_i), \tag{6}$$

where the product runs over all individual parameters i.
The prior on each parameter is to be specified by the user, using the large variety of distributions available in the scipy.stats[3] module (Virtanen et al. 2020).

The resulting posterior distribution, $p(\vartheta|D)$, is then sampled using MCMC. More specifically, we use the affine-invariant ensemble sampling implementation of the emcee library Foreman-Mackey et al. (2019). Convergence of the walkers is monitored at regular intervals based on the autocorrelation length of the chains, using the following algorithm. Every $n_{\rm check}$ steps (*i.e.* accepted positions in the parameter space), the integrated autocorrelation length τ_j of each chain j is computed, as well as the average autocorrelation over all chains, $\tau = \langle \tau_j \rangle$. Convergence is accepted if both of the two following criteria are met:

1. The current length of the chains is longer than $n_{\rm auto} \times \tau$;
2. The mean autocorrelation has changed by less than $\Delta\tau_{\rm max}$ in the last two evaluations.

The values of $n_{\rm auto}$ and $\Delta\tau_{\rm max}$ are parameters of panco2, that need to be specified by the user. Likewise, the user needs to provide a maximum chain length at which the sampling should stop if convergence was never reached.

2.6. *Chains cleaning and exploitation*

Once MCMC convergence has been reached, panco2 stores the full sampling of the posterior distribution, *i.e.* all of the accepted positions in the parameter space and their associated log-likelihood and log-posterior values. The raw chains can then be loaded and cleaned as follows:

1. Remove the first $n_{\rm burn}$ samples as a burn-in length;
2. Thin the chains by discarding $(n_{\rm discard} - 1)/n_{\rm discard}$ samples, *i.e.* only keeping one sample every $n_{\rm discard}$ steps;
3. Discard the chains that are poorly mixed, *i.e.* systematically outside of the $[q_{\rm extr}, 1 - q_{\rm extr}]$ quantiles of the sampled posterior.

[3] https://docs.scipy.org/doc/scipy/reference/stats.html

Again, the values of $n_{\rm burn}$, $n_{\rm discard}$ and $q_{\rm extr}$ are parameters of the analysis, that must be user-provided.

The cleaned chains can then be expressed in the pressure profile space. To do so, eq. (1) is used to compute a profile for each position in the parameter space, over a radial range specified by the user. These profiles may then be saved for future analyses.

The Markov chains, in the parameter space and in the pressure profile space, constitute the main data product of panco2. Several figures can be produced for a visual representation of the results. They are all presented in the technical documentation **[todo: add link]**; we give here a brief description of these figures.

Posterior distribution — Several functions are available to produce figures showing properties of the Markov chains and the posterior distribution they sample, using the ChainConsumer library (Hinton 2016):

- Walks plot, *i.e.* the evolution of the positions in the parameter space with the number of steps for each parameter;
- Corner plot, *i.e.* a figure showing the marginalized posterior for all individual parameters and sets of two parameters. The prior distribution can be overplotted for comparison purposes;
- Plot of the correlation and covariance matrices of the different parameters.

Data – Model – Residuals — Two figures can be produced to illustrate the quality of the fit. They both consist in comparing the input data, the best-fitting model, and the residuals (*i.e.* the difference between input data and best-fitting model). These can be plotted in 2D, by showing the three maps side-by-side (see figure 4), or in 1D, by showing the radial profiles of each of these maps in the same graph (see the left panels of figure 5). Goodness of fit can be judged in both representations by lack of significant structure in the residuals.

Pressure profile — In addition, a plot of the median of these profiles, as well as confidence intervals chosen as their 16th and 84th percentiles, can be produced (see the right panels of figure 5).

3. VALIDATION ON SIMULATIONS

In order to ensure that panco2 is able to recover accurate pressure profile measurements, we test it on simulated inputs. In this section, we detail this validation process, from the creation of the dataset to the results produces by panco2. For reproducibility purposes, the datasets created and used for this analysis are made public with the software.

3.1. *Sample selection*

The goal of the validation is to ensure that panco2 is able to recover accurate pressure profiles from different types of data. To that end, we seek to create realistic synthetic cluster maps from three instruments: the *Planck* satellite, the South Pole Telescope (SPT), and the NIKA2 camera at the IRAM 30 m telescope. The choice of these three instruments is motivated by their vastly different angular resolutions: the Compton−y maps built from *Planck* and SPT data have angular resolutions (expressed as the full width at half maximum, or FWHM) of 10 and 1.25 arcmin, respectively (Planck Collaboration et al. 2016b; Bleem et al. 2022), and the beam of the NIKA2 camera

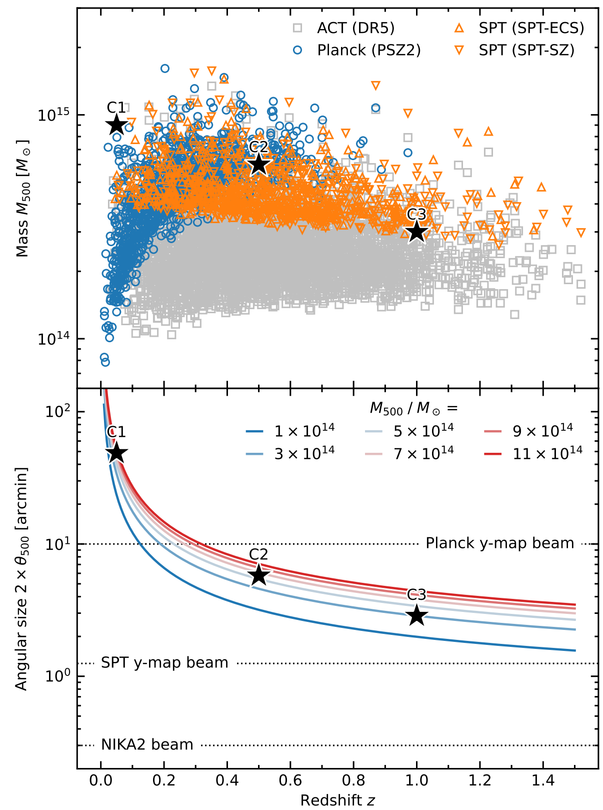

FIG. 3.— Validation cluster sample (black stars) in the mass-redshift plane (*top panel*) and in the angular size-redshift plane (*bottom panel*). For illustration, the top panel includes clusters detected in recent tSZ surveys: *Planck* (Planck Collaboration et al. 2016a), ACT (Hilton et al. 2021), and SPT (Bleem et al. 2020, 2015). Note that the redshift axis is truncated to $z < 1.6$, therefore not showing all clusters in these samples. Colored lines in the bottom panel show the evolution of the angular $2 \times \theta_{500}$ with redshift for clusters of different masses. The angular resolutions of the *Planck* and SPT y−maps, as well as that of the NIKA2 camera at 150 GHz, are represented as dotted horizontal lines.

150 GHz band – used for tSZ mapping – has an FWHM of 18 arcsec (Perotto et al. 2020).

We choose to create SZ maps for three clusters, labeled (C1, C2, C3), covering different regions of the mass-redshift plane:

$$\begin{aligned} \text{C1}: z = 0.05,\ & M_{500} = 9 \times 10^{14}\ M_\odot; \\ \text{C2}: z = 0.5,\ & M_{500} = 6 \times 10^{14}\ M_\odot; \\ \text{C3}: z = 1,\ & M_{500} = 3 \times 10^{14}\ M_\odot, \end{aligned} \tag{7}$$

These mock clusters are shown as black stars in figure 3. The top panel shows their positions in the mass-redshift plane, indicating that C1, C2 and C3 are realistic detections for the *Planck*, SPT, and ACT tSZ surveys, respectively. Tbe bottom panel of figure 3 places the clusters in the angular diameter-redshift plane, showing that C1 can be resolved in *Planck*, SPT, and NIKA2 tSZ maps, while C2 and C3 are too small to be resolved by *Planck*.

3.2. *Data generation*

We create mock maps for the three clusters by forward modeling their tSZ signal. We assume that each cluster has a pressure profile that follows the universal profile of A10, scaled with its mass and redshift. This pressure distribution is in-

Instrument (Clusters)	Map size $\theta_{\rm map}$	Pixel size $\theta_{\rm pix}$	FWHM $\theta_{\rm FWHM}$	Filtering	White noise level
Planck (C1)	$5°$	$2'$	$10'$	–	Homogeneous RMS=4.12×10^{-6} $[y]$
SPT (C1, C2)	$30'$	$15''$	$1.25'$	–	Homogeneous, RMS=9.78×10^{-6} $[y]$
NIKA2 (C2, C3)	$6.5'$	$3''$	$18''$	NIKA2-like transfer function	Isotropic NIKA2-like RMS

TABLE 1
Properties of simulated maps emulating cutouts of the *Planck* (Planck Collaboration et al. 2016b) and SPT (Bleem et al. 2022) $y-$maps, and NIKA2 cluster observations (Kéruzoré et al. 2020).

tegrated along the line of sight to obtain a Compton$-y$ map. This map is then projected on a flat-sky grid and convolved with a Gaussian filter to account for instrumental filtering, and added to a random noise realization.

As discussed previously, and illustrated in the bottom panel of figure 3, the angular size of each cluster is very different, and the mapping of their tSZ signal is very different for all instruments considered. We therefore create different sets of maps for the three clusters. For C1, the most extended cluster, we create mock *Planck* and SPT maps. For C2, our intermediate case, we create SPT and NIKA2 mock maps. Finally, for C3, the smallest cluster in our sample, we only create mock NIKA2 data. The characteristics of the maps are designed to mimic know cluster observations by the three instruments, and summarized in table 1. The generated maps are shown on the left panels of figure 4.

Planck-like data — Our mock *Planck* dataset is designed to emulate the *Planck* `MILCA` Compton$-y$ map of Planck Collaboration et al. (2016b). The original data products for this map are in `healpix` format, which `panco2` cannot process, as it relies on the flat-sky approximation. We therefore create maps of $(5° \times 5°)$ patches of the sky using a gnomonic projection, with a pixel size of $2'$, and a Gaussian PSF of FWHM = $10'$. The noise in these maps is white and has an homogeneous distribution, with an RMS taken from the left panel of figure 13 in Planck Collaboration et al. (2016b). We do not consider any filtering of the signal aside from the beam convolution, as the scales filtered out by the data processing are very large compared to the size of the patch considered (see Planck Collaboration et al. 2016b).

SPT-like data — Our SPT-like maps mimic the publicly available $y-$map released by the SPT collaboration (Bleem et al. 2022), specifically the "minimum variance" map. We use the same projection as their flat-sky maps, *i.e.* a Sanson-Flamsteed projection with $15''$ pixels, on a $(30' \times 30')$ patch of the sky. The resolution of the maps is Gaussian with FWHM = $1.25'$. We inject white noise realizations, the amplitude of which is evaluated by computing the RMS of the map in a $(5°\times5°)$ patch of the sky, taking care of masking sources. The SPT $y-$maps use information from the *Planck* $y-$map in the Fourier space to compensate for large-scale filtering, making it negligible ($< 8\%$ filtering for angular scales $\ell < 2 \times 10^4$). Therefore, we choose to consider no filtering in the creation of these maps.

NIKA2-like data — Our NIKA2-like data imitates the NIKA2 150 GHz sky maps obtained by the NIKA2 SZ Large Program (Mayet et al. 2020; Perotto et al. 2021). In particular, we use the data products publicly released in Kéruzoré et al. (2020). We create a gnomonic projection of a $(6.5' \times 6.5')$ patch of the sky with $3''$ pixels. The angular resolution of the map is Gaussian with FWHM = $18''$, and we also take into account filtering of angular scales due to data processing via the transfer function of Kéruzoré et al. (2020). The noise in these NIKA2 maps is considered white and isotropic, but not homogeneous, as the NIKA2 on-the-fly scanning strategy used for obsevations of the NIKA2 SZ Large Program creates a variation in the noise level of the maps depending on the distance from the pointing coordinates. To accurately take into account this effect, we use the noise RMS map of Kéruzoré et al. (2020), which we multiply by a scalar value to account for different exposure times. Data produced by the NIKA2 collaboration is in NIKA2 150 GHz surface brightness units, usually presented in mJy/beam. The conversion coefficient of y-to$-$mJy/beam can be evaluated by integrating the tSZ spectral distortion in the NIKA2 150 GHz effective bandpass (accounting for atmospheric opacity at the time of the observations), and is usually of the order of -12 mJy/beam/y (*e.g.* Kéruzoré et al. 2020), therefore we choose this value for our map generation.

3.3. *Pressure profile fitting*

The five generated maps are then used to extract a pressure profile using `panco2`, *i.e.* following the procedure detained in §2. We assume that we know the characteristics of the map prior to fitting – *i.e.* the width of the beams used, the transfer function, and the noise RMS given to `panco2` in input are the same ones that have beed used to generate the maps.

Two ingredients in our model then remain to be specified: the radial binning – *i.e.* the value of the radii R_i in eq.(1) – and the priors on the parameters. For the radial binning, we choose one that is identically determined by the angular coverage of each map. The first bin is defined as the projected radius corresponding to the size of a map pixel, $R_0 = \mathcal{D}_{\rm A}(z) \tan^{-1} \theta_{\rm pix}$, where $\mathcal{D}_{\rm A}(z)$ is the angular diameter distance to the cluster redshift z. Four bins $\{R_1 \dots R_4\}$ are then added, log-spaced between the projected sizes of the beam FWHM, $\mathcal{D}_{\rm A}(z) \tan^{-1} \theta_{\rm FWHM}$, and of the half map size, $\mathcal{D}_{\rm A}(z) \tan^{-1} \theta_{\rm map}/2$.

The priors on each parameter is defined as follows. For the pressure parameters P_i, corresponding to the value of the pressure profile at radii R_i, we compute the value of the universal pressure profile from A10 for the cluster's mass and redshift. The prior on P_i is then set as a log-uniform distribution around this value:

$$p(P_i) = \log \mathcal{U}(10^{-2}, 10^2) \times P_{\rm A10}(R_i). \quad (8)$$

The prior on the conversion coefficient is set as a Gaussian distribution. For *Planck*- and SPT-like maps, the data is directly in units of Compton$-y$, therefore this distribution is centered around 1. For NIKA2 data, as discussed in §3.2, the central value of the prior is set at -12 mJy/beam/y. For all data, the spread of the distribution is taken as 5% of its central value.

The MCMC sampling is run as presented in §2.5, with 30 walkers, and setting $n_{\rm auto} = 50$ and $\Delta\tau_{\rm max} = 5\%$. For our tests, we used a 2021 MacBook Pro with an M1 Pro chip and a 10-core CPU, with the MCMC using 5 threads **[todo: is this necessary?]**. With this setup and these criteria, each fit took 5 to 10 minutes to converge. The raw Markov chains are then saved, and cleaned for the exploitation as described in §2.6, with $n_{\rm burn} = 500$, $n_{\rm discard} = 20$, and $q_{\rm extr} = 20\%$.

3.4. *Results*

The results of the regression is presented in Figures 4 and 5. Figure 4 shows, for each of the five datasets, the simulated data (left), best-fitting 2D model (center), and the residuals (right). The residuals panels show no significant structure, providing a visual indication of goodness of fit. The right panels of Figure 5 also shows the data, model, and residuals, but as 1D azimuthal profiles, and include uncertainty computed from the spread of the sampled posterior. The compatibility of the green curves (*i.e.* residuals) with zero within uncertainties proves that `panco2` is able to retrieve a pressure profile that fits the data.

The left panels of Figure 5 show the pressure profiles recovered for each fit as the blue curves, including uncertainties. The true profile used to generate each map data (*i.e.* the universal A10 pressure profile for the cluster's mass and redshift, see §3.2) is shown as a black dashed line. For each data set, the agreement between the two curves across the considered radial range (*i.e.* from the projected pixel size to the projected half map size) shows that `panco2` is able to retrieve an accurate estimation of the pressure profile of a cluster from its tSZ map.

4. ADDITIONAL SIMULATED DATASETS

The simulations described in §3 did not feature all the possibilities of pressure profile fitting offered by `panco2`. To extend the validation to these different analysis options, we create additional datasets, based on the same mock clusters and instrumental data coverages, but each featuring one more component to the modeling.

4.1. *Correlated noise*

We create a mock SPT map of the C2 galaxy cluster featuring realistic correlated noise. We evaluate the power spectrum of noise in the SPT y−map from a $(5^\circ \times 5^\circ)$ patch of the minimum variance map published in Bleem et al. (2022), in which astrophysical sources were masked. The power spectrum is used to create 10^4 random noise realizations, that are used to compute the covariance matrix of the noise in map pixels. One of these noise realizations is added to the simulated tSZ signal, and the inverted noise covariance is used in the likelihood function of eq. (3).

The pressure profile fitting is performed the same way as described in §3.3. The results are presented in figure **[todo: .]**

4.2. *Two-dimensional transfer function*

We create a mock SPT map of the C1 galaxy cluster featuring anisotropic filtering by a two-dimensional transfer function. Even though the published SPT y−maps have negligible filtering (see Bleem et al. 2022), single-band SPT maps are created with a **[todo: very anisotropic transfer function to describe]**. We create a mock map featuring an artificial anisotropic filtering mimicking this transfer function, which is accounted for in the forward modeling of the tSZ map.

Results are shown in figure **[todo: .]**

4.3. *Point source contamination*

We generate a mock NIKA2 map of the C2 cluster in which point sources are added to the surface brightness map. We choose to add two point sources S1 and S2, each with a flux of $F = 1$ mJy, and respectively located at 30″ and 75″ from the cluster center. They are added to the sky model with their true positions, and fluxes are treated as a model parameter as described in §2.3.

The fitting is performed the same way as described in §3.3. Priors on their fluxes are added as a Gaussian distribution for S1, with $p(F_1) = \mathcal{N}(1\,\mathrm{mJy}, 0.2\,\mathrm{mJy})$, and as an uniform distribution for S2, corresponding to an upper limit on the flux, with $p(F_2) = \mathcal{U}(0\,\mathrm{mJy}, 2\,\mathrm{mJy})$. The results are presented in figure **[todo: .]**

4.4. *Integrated SZ signal constraint*

Finally, we run the fit of the mock NIKA2 map of the C2 cluster discussed in §3 with an added constraint on its integrated tSZ signal, as described in §2.4. We use the $Y - M$ scaling relation of Arnaud et al. (2010) to compute an estimated value of Y_{500} (corresponding to the integrated tSZ signal within R_{500}) of Y_{500} =**[todo: .]** We consider an uncertainty of 10%. The additional constrain is added to the log-likelihood using eq. (5).

Results are presented in **[todo: .]**

5. CONCLUSIONS AND DISCUSSION

This paper presents the release of `panco2`, a software enabling its users to perform pressure profile extraction from a tSZ map. We have presented the main features of the software, based on forward modeling MCMC of the tSZ signal with a radially-binned pressure profile. We have presented the variety of observational systematics that can be incorporated in the modeling in order to account for the known features of millimeter-wave observations. In section §3, we have shown that `panco2` could retrieve unbiased pressure profile estimates from *Planck*-like, SPT-like, and NIKA2-like data, effectively covering a range of angular resolutions from 18″ to 10′. The software is made public, along with a detailed documentation providing deeper technical insights on the code and its usage.

5.1. *Products released*

The entirety of the `panco2` software is made available as a github repository[4]. That same repository also includes the data generated for the validation described in §3, along with the products of said validation (*i.e.* the Markov chains and the running sequences used for each dataset). Alternatively, `panco2` can be installed through `pip` as follows **[todo: not true yet]**:

```
$ pip install panco2
```

In addition, `panco2` is also accompanied by an online technical documentation **[todo: url]**. It includes detailed explanations of the technical aspects of the code, as well as a description of the inputs and outputs of `panco2`'s different functions. The documentation also gives examples of analyses that can be performed with `panco2` beyond the ones presented in the validation.

[4] https://github.com/fkeruzore/panco2

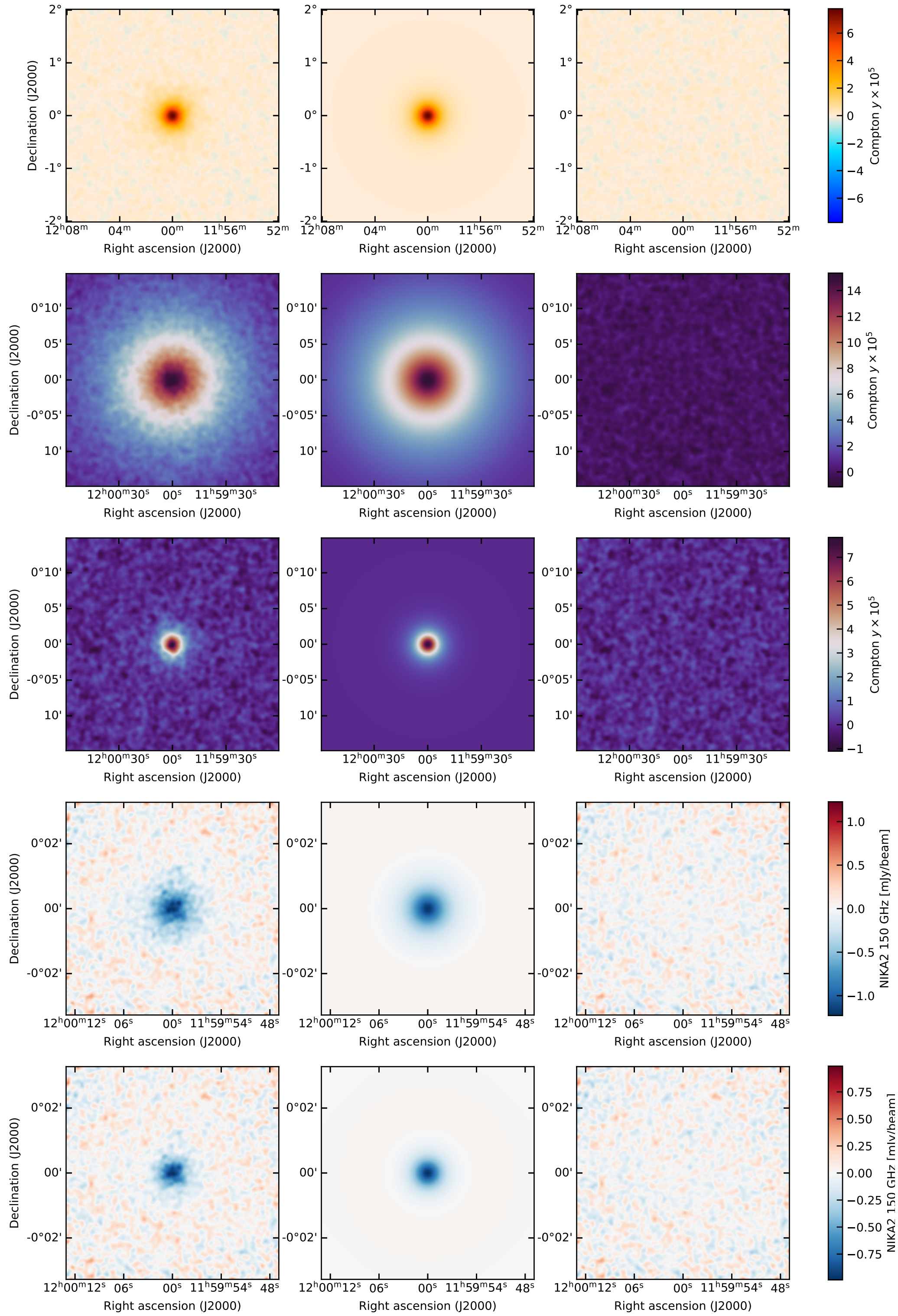

FIG. 4.— Data (*left*), model (*center*), and residuals (*i.e.* difference between data and model, *right*) for the five validation fits: from top to bottom, C1 with *Planck*, C1 with SPT, C2 with SPT, C2 with NIKA2, C3 with NIKA2. Maps are smoothed by a 1 pixel Gaussian for display purposes.

5.2. *Possible future improvements*

This release of panco2 allows a user to perform the fit of a radially binned pressure profile model on a tSZ map. Several additional features can be thought of to offer more flexibility in this kind of analysis. Here, we offer a non-exhaustive list of possible such extensions. We strongly emphasize that this list should *not* be interpreted as a list of features currently in development by the authors, but instead as a collection of possible avenues to explore.

Joint analysis of several tSZ maps — We have shown in §3 that panco2 could recover pressure profiles from tSZ observations with different kinds of instruments – namely, we have tested *Planck*-, SPT-, and NIKA2-like mappings. But our analysis treated all of these datasets separately. For clusters with available data from several instruments, there may be interesting information to be extracted from the joint analysis of several maps (see *e.g.* Ruppin et al. 2018; Romero et al. 2018).

Different profile parametrizations — As discussed in §2.2, many studies of pressure profiles from tSZ (or X-rays) observations use the gNFW profile. Even though our radially-binned parametrization offers more flexibility and circumvents the known problems of the usual gNFW parametrization, one may be interested in using other functional forms of pressure profile. For example, the rewriting of the gNFW model from Battaglia et al. (2012) (see also *e.g.* Sayers et al. 2022) offers a way to constrain the same functional form, but minimizing the correlations in the parameter space. Even though it is still possible to use a radially-binned profile and to fit any other functional form on the pressure bins *a posteriori* (see *e.g.* Muñoz-Echeverría et al. 2022a), one may want to directly fit said parametrization to the data, which is currently not supported.

Non-spherical pressure models — Galaxy clusters are well known to not be perfectly spherical structures. Consequently, fitting a spherically-symmetric pressure distribution misses some information potentially contained in tSZ maps. For examples, clusters can be aspherical because they are an ongoing merger of two substructures. Observations of such systems can give precious insights on the dynamics of cluster mergers, and therefore on the physics of large-scale structure formation. Additionally, non-merging clusters may be aspherical because of their connection to the cosmic web, which can provide interesting insights on cosmic filaments. Therefore, the possibility to fit pressure distributions beyond spherical symmetry is interesting. Depending on the morphology of the system, this may be done by fitting for an ellipsoidal pressure distribution (*e.g.* Sarazin et al. 2016), or the sum of the contributions of two (possibly spherical) halos (*e.g.* Artis et al. 2022). These possibilities are not implemented in panco2, but might be an interesting extension.

Joint tSZ–X-ray analysis — The *bremsstrahlung* of hot electrons makes the ICM emit in the X-ray domain (see *e.g.* Böhringer & Werner 2010; Böhringer & Schartel 2013, for reviews). This radiation carries information on the ICM that is very complementary to that offered by tSZ observations. Namely, similarly to how tSZ signal is linked to the electron pressure in the ICM – as seen in eq. (2) – X-ray emission is linked to its (squared) electron density. Moreover, for sufficiently deep observations, X-ray data can also be used to study the spectral distribution of the detected photons, enabling measurements of the ICM electron temperature. The combination of X-ray and tSZ observations of clusters therefore offers a way to finely characterize ICM thermodynamics. This complementarity can be exploited *a posteriori*, *e.g.* by combining results from panco2 with density and temperature profiles obtained independently of X-ray data (*e.g.* Kéruzoré et al. 2020), or through a joint fit of the thermodynamic properties (*e.g.* Castagna & Andreon 2020). The possibility of joint tSZ–X-ray fits could be added to panco2 to take further advantage of this complementarity.

5.3. *Recommendations to users*

[todo: this is a terrible section title, please help]

As discussed in §2.2, the pressure model fitted on the data requires the user to define a set of radii used as nodes for the power-law interpolation of the profile. The choice of these radii is far from straightforward, as it depends on the angular scales present in the data to be fitted, as well as on the scientific goals of the analysis. This is the main downside of the radially binned model used in panco2, as the radii chosen may have a significant impact on the analysis results. The model dependence of products derived from radially-binned pressure profiles has been discussed by Muñoz-Echeverría et al. (2022a), who show that hydrostatic mass estimates, linked to the first derivative of the pressure profile, are particularly affected.

In order to try to circumvent this shortcoming, we strongly advise panco2 users to be cautious about their choice of binning, and, when possible, to try different binnings. We have implemented functions in panco2 that allow users to easily simulate a mock tSZ map mimicking the data to be fitted. We encourage users to use this functionality to create such datasets and try out their choices of radial binning on these. Similarly to the validation presented in §3.4, the comparison of the pressure profile reconstructed with the one used to generate the map will provide insights on how well adapted a choice of radial binning is to a dataset. How to perform such an analysis is presented in the technical documentation, at **[todo: url]**.

ACKNOWLEDGEMENTS

The development of panco2 comes after many years of work on pressure profile fitting codes within the NIKA2 collaboration, for which we acknowledge major contributions by R. Adam and C. E. Romero. Argonne National Laboratory's work was supported by the U.S. Department of Energy, Office of Science, Office of High Energy Physics, under contract DE-AC02- 06CH11357.

REFERENCES

Adam, R., Adane, A., Ade, P. a. R., et al. 2018, A&A, 609, A115, doi: 10.1051/0004-6361/201731503
Allen, S. W., Evrard, A. E., & Mantz, A. B. 2011, Annu. Rev. Astron. Astrophys., 49, 409, doi: 10.1146/annurev-astro-081710-102514
Arnaud, M., Pratt, G. W., Piffaretti, R., et al. 2010, A&A, 517, A92, doi: 10.1051/0004-6361/200913416
Artis, E., Adam, R., Ade, P., et al. 2022, 257, 00003, doi: 10.1051/epjconf/202225700003
Battaglia, N., Bond, J. R., Pfrommer, C., & Sievers, J. L. 2012, The Astrophysical Journal, 758, 75, doi: 10.1088/0004-637X/758/2/75
Bleem, L. E., Stalder, B., de Haan, T., et al. 2015, ApJS, 216, 27, doi: 10.1088/0067-0049/216/2/27
Bleem, L. E., Bocquet, S., Stalder, B., et al. 2020, ApJS, 247, 25, doi: 10.3847/1538-4365/ab6993
Bleem, L. E., Crawford, T. M., Ansarinejad, B., et al. 2022, The Astrophysical Journal Supplement Series, 258, 36, doi: 10.3847/1538-4365/ac35e9

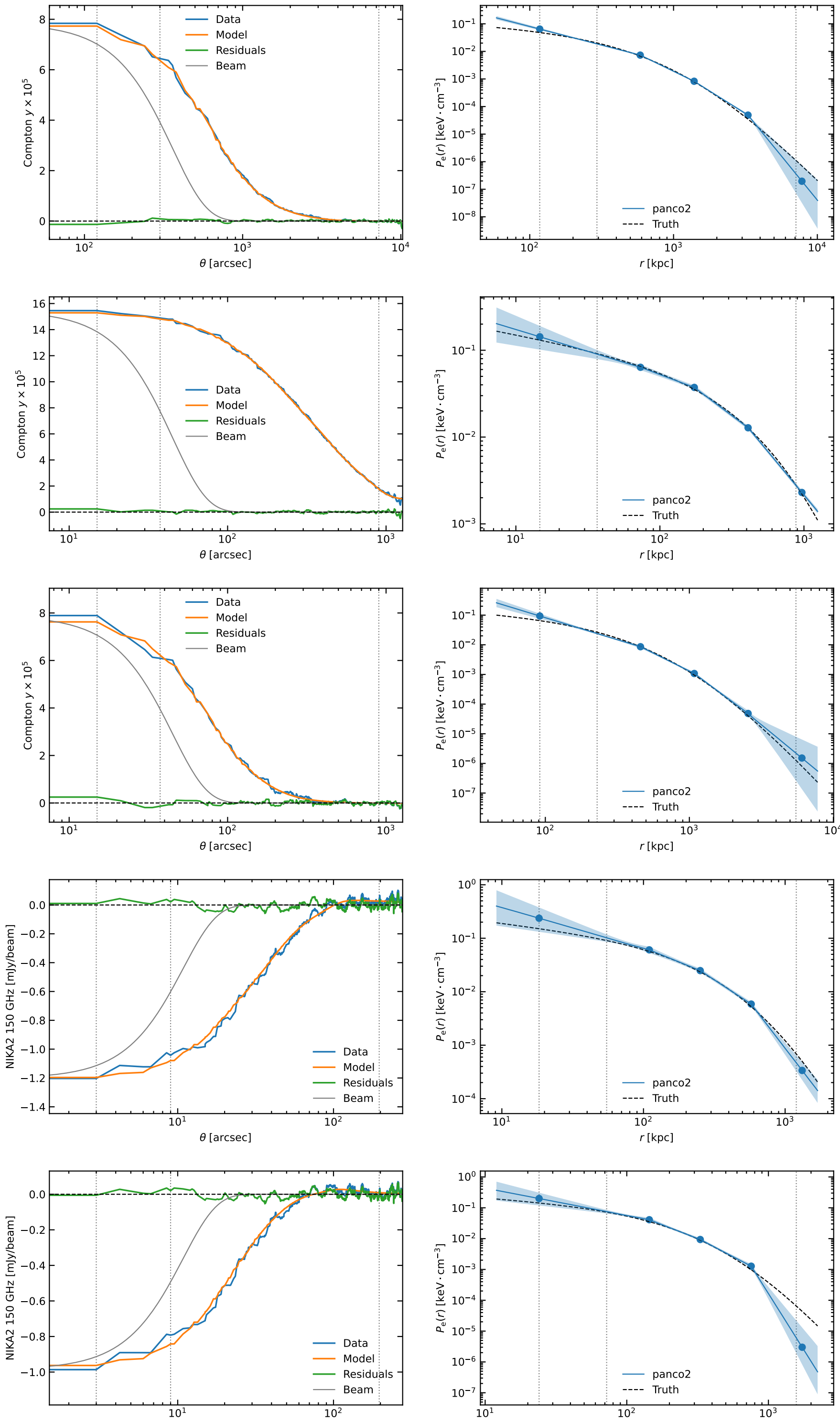

FIG. 5.— **Left:** Data, model, and residuals (*i.e.* difference between data and model) azimuthal profiles for the five validation fits. The beam profile is shown in grey for comparison. The rows are identical to Figure 4. **Right:** Pressure profiles reconstructed for each validation fit (blue line). For each profile, the shaded area marks the region between the 16th and 84th percentiles of the posterior distribution. The dashed black line shows the true pressure profile used to generate each map. In each plot, dotted vertical lines, from left to right, show the size of a map pixel, the beam HWHM, and the half map size.

Böhringer, H., & Schartel, N. 2013, Astronomische Nachrichten, 334, 482, doi: 10.1002/asna.201211886
Böhringer, H., & Werner, N. 2010, Astron Astrophys Rev, 18, 127, doi: 10.1007/s00159-009-0023-3
Carlstrom, J. E., Holder, G. P., & Reese, E. D. 2002, Annual Review of Astronomy and Astrophysics, 40, 643, doi: 10.1146/annurev.astro.40.060401.093803
Castagna, F., & Andreon, S. 2020, Astronomy & Astrophysics, 639, A73, doi: 10.1051/0004-6361/202037543
DES Collaboration, Abbott, T. M. C., Aguena, M., et al. 2020, Phys. Rev. D, 102, 023509, doi: 10.1103/PhysRevD.102.023509
Di Mascolo, L., Churazov, E., & Mroczkowski, T. 2019, Monthly Notices of the Royal Astronomical Society, 487, 4037, doi: 10.1093/mnras/stz1550
Foreman-Mackey, D., Farr, W., Sinha, M., et al. 2019, The Journal of Open Source Software, 4, 1864, doi: 10.21105/joss.01864
Hilton, M., Sifón, C., Naess, S., et al. 2021, The Astrophysical Journal Supplement Series, 253, 3, doi: 10.3847/1538-4365/abd023
Hinton, S. R. 2016, The Journal of Open Source Software, 1, 00045, doi: 10.21105/joss.00045
Kéruzoré, F., Artis, E., Macías-Pérez, J.-F., et al. 2021, EPJ Web of conferences, 257, 00024. https://arxiv.org/abs/2111.06493
Kéruzoré, F., Mayet, F., Pratt, G. W., et al. 2020, A&A, 644, A93, doi: 10.1051/0004-6361/202038933
Liu, A., Bulbul, E., Ghirardini, V., et al. 2022, A&A, 661, A2, doi: 10.1051/0004-6361/202141120
Mayet, F., Adam, R., Ade, P., et al. 2020, EPJ Web Conf., 228, 00017, doi: 10.1051/epjconf/202022800017
Melin, J.-B., Aghanim, N., Bartelmann, M., et al. 2012, Astronomy and Astrophysics, 548, A51, doi: 10.1051/0004-6361/201015689
Mroczkowski, T., Nagai, D., Basu, K., et al. 2019, Space Science Reviews, 215, 17, doi: 10.1007/s11214-019-0581-2
Muñoz-Echeverría, M., Macías-Pérez, J., Pratt, G. W., Adam, R., & Ade, P. 2022a, in prep.
Muñoz-Echeverría, M., Adam, R., Ade, P., et al. 2022b, 257, 00033, doi: 10.1051/epjconf/202225700033
Nagai, D., Kravtsov, A. V., & Vikhlinin, A. 2007, ApJ, 668, 1, doi: 10.1086/521328
Perotto, L., Ponthieu, N., Macías-Pérez, J. F., et al. 2020, A&A, 637, A71, doi: 10.1051/0004-6361/201936220
Perotto, L., Adam, R., Ade, P., et al. 2021, EPJ Web of conferences, 257, 00038. https://arxiv.org/abs/2111.01729
Planck Collaboration, Ade, P. a. R., Aghanim, N., et al. 2013, A&A, 550, A131, doi: 10.1051/0004-6361/201220040
—. 2016a, A&A, 594, A27, doi: 10.1051/0004-6361/201525823
Planck Collaboration, Aghanim, N., Arnaud, M., et al. 2016b, A&A, 594, A22, doi: 10.1051/0004-6361/201525826
Romero, C., McWilliam, M., Macías-Pérez, J.-F., et al. 2018, A&A, 612, A39, doi: 10.1051/0004-6361/201731599
Romero, C. E., Mason, B. S., Sayers, J., et al. 2017, ApJ, 838, 86, doi: 10.3847/1538-4357/aa643f
Romero, C. E., Sievers, J., Ghirardini, V., et al. 2020, The Astrophysical Journal, 891, 90, doi: 10.3847/1538-4357/ab6d70
Ruppin, F., Mayet, F., Macías-Pérez, J. F., & Perotto, L. 2019, Monthly Notices of the Royal Astronomical Society, 490, 784, doi: 10.1093/mnras/stz2669
Ruppin, F., Mayet, F., Pratt, G. W., et al. 2018, A&A, 615, A112, doi: 10.1051/0004-6361/201732558
Sarazin, C. L., Finoguenov, A., Wik, D. R., & Clarke, T. E. 2016, arXiv e-prints, 1606, arXiv:1606.07433
Sayers, J., Mantz, A. B., Rasia, E., et al. 2022, The Evolution and Mass Dependence of Galaxy Cluster Pressure Profiles at 0.05 $\le z \le$ 0.60 and $4 \times 10{14}$ M$_{\odot}$ $\le \textrm{M}_{500} \le 30 \times 10{14}$ M$_{\odot}$
Sunyaev, R. A., & Zeldovich, Y. B. 1972, Comments on Astro. and Space Physics, 4, 173
—. 1980, Monthly Notices of the Royal Astronomical Society, 190, 413, doi: 10.1093/mnras/190.3.413
Virtanen, P., Gommers, R., Oliphant, T. E., et al. 2020, Nature Methods, 17, 261, doi: 10.1038/s41592-019-0686-2
Wells, D. C., Greisen, E. W., & Harten, R. H. 1981, Astronomy and Astrophysics Supplement, Vol. 44, P. 363, 1981, 44, 363
Young, M., et al. 2022, in prep.
Zhao, H. 1996, Monthly Notices of the Royal Astronomical Society, 278, 488, doi: 10.1093/mnras/278.2.488

APPENDIX

A. SOME APPENDIX?

Lorem ipsum dolor sit amet, consectetuer adipiscing elit. Ut purus elit, vestibulum ut, placerat ac, adipiscing vitae, felis. Curabitur dictum gravida mauris. Nam arcu libero, nonummy eget, consectetuer id, vulputate a, magna. Donec vehicula augue eu neque. Pellentesque habitant morbi tristique senectus et netus et malesuada fames ac turpis egestas. Mauris ut leo. Cras viverra metus rhoncus sem. Nulla et lectus vestibulum urna fringilla ultrices. Phasellus eu tellus sit amet tortor gravida placerat. Integer sapien est, iaculis in, pretium quis, viverra ac, nunc. Praesent eget sem vel leo ultrices bibendum. Aenean faucibus. Morbi dolor nulla, malesuada eu, pulvinar at, mollis ac, nulla. Curabitur auctor semper nulla. Donec varius orci eget risus. Duis nibh mi, congue eu, accumsan eleifend, sagittis quis, diam. Duis eget orci sit amet orci dignissim rutrum.

This paper was built using the Open Journal of Astrophysics LaTeX template. The OJA is a journal which provides fast and easy peer review for new papers in the astro-ph section of the arXiv, making the reviewing process simpler for authors and referees alike. Learn more at http://astro.theoj.org.